Refractive index enhancement with vanishing absorption in short, high-density vapor cells

Z. J. Simmons, N. A. Proite, J. Miles, D. E. Sikes, and D. D. Yavuz
Department of Physics, 1150 University Avenue, University of Wisconsin at Madison, Madison, Wisconsin 53706, USA
(Received 19 March 2012; published 9 May 2012)

It has recently been predicted and experimentally demonstrated that the refractive index of a vapor may be enhanced while maintaining vanishing absorption by using the interference of two Raman transitions, one absorptive and one amplifying in nature. In this paper, we present a detailed experimental study of this technique in a 1-mm-long rubidium (Rb) vapor cell with densities exceeding 10^{14} cm^{-3}. We study the optimization of the achieved refractive index as various experimental parameters are varied and discuss a number of limitations of the current experiments. We also present a detailed discussion of possible experimental improvements and future prospects of this technique.

DOI: 10.1103/PhysRevA.85.053810 PACS number(s): 42.50.Gy, 42.65.An, 42.65.Dr, 78.20.Ci

Laser physicists strive to engineer the optical response of materials. Naturally available materials, such as atomic gases in thermal equilibrium, offer only a limited set of optical properties. For many experiments and practical applications, the optical response needs to be controlled to produce a desired effect on a propagating light wave. Over the last two decades, a number of techniques have been demonstrated that alter the atomic response to near-resonant light. For example, using electromagnetically induced transparency (EIT), one can render transparent an otherwise opaque medium to a resonant laser beam [1–3]. It is now understood that using EIT and similar techniques, one can obtain slow light [4–8], stopped light [9–13], and construct optical nonlinearities that are large enough to be effective at the single-photon level [14–24]. These effects have had a big impact on our understanding of the fundamental physics behind light-matter interactions. Furthermore, observation of these effects has opened up a number of exciting applications across a variety of fields including quantum computing and all-optical information processing.

Despite this great progress, a key aspect of these studies has remained elusive. EIT and related techniques utilize the steep dispersion (the slope) of the refractive index as a function of frequency. An effective scheme that allows us to engineer the value of the refractive index has not yet been developed. Over the last two decades, a number of techniques that manipulate the refractive index without increasing absorption have been suggested. The field started with the pioneering work of Scully [25,26], which was later extended by a number of authors [27–29]. In this paper, we focus on the recent suggestion of using the interference of two far-off-resonant Raman transitions for enhancing the refractive index while maintaining vanishing absorption [30,31]. We recently reported a proof-of-principle experiment in low-density rubidium (Rb) vapor that demonstrated the key ideas of this technique [32]. In the present work, we extend this experiment to short alkali-metal vapor cells with densities exceeding 10^{14} cm^{-3}, that is, densities more than two orders of magnitude higher than what has typically been used in EIT experiments. We present a detailed study of the strength of the Raman resonances as a function of various experimental parameters such as the single-photon detuning, the cell temperature, and the intensity of the control lasers. We also report a study of F-level specific optical pumping at high vapor densities, which is critical for our studies of index enhancement. Our experiments demonstrate relative refractive index values of $\Delta n \approx 10^{-4}$, which is more than two orders of magnitude larger than in our earlier proof-of-principle experiment.

A key practical application of index enhancement schemes is optical imaging science. As the frontiers of science and engineering approach the nanoscale, it becomes ever more important to devise optical imaging techniques with nanometer resolution. It is well known that the resolution of a traditional optical imaging system is limited by the wavelength of light. This is the diffraction limit, and overcoming this barrier has been the subject of intense theoretical and experimental research [34–41]. The wavelength of light inside a refractive medium is $\lambda = \lambda_0/n$, where λ_0 is the wavelength in vacuum. A large refractive index, therefore, corresponds to a reduced wavelength inside the medium and enhanced imaging resolution. Similarly, because of the reduced wavelength, the lower limit on feature size of a lithographic mask is reduced in a high index medium. This is particularly important since lithographic resolution currently determines the size and the processing power of every semiconductor integrated circuit.

I. INTRODUCTION

It is well known that a laser beam tuned close to an atomic resonance can experience a large refractive index. However, such a large index is usually accompanied by large absorption. It was first pointed out by Scully [25,26] that, using atomic coherence, it is possible to obtain a large refractive index with negligible absorption. The pioneering work of Scully was extended to different configurations by Fleischhauer and colleagues [27–29]. Although these ideas were experimentally demonstrated in an Rb vapor cell by Zibrov *et al.* [33], a refractive index in a vapor that is large enough to be of practical importance has yet to be achieved.

Building on these pioneering efforts, our approach utilizes the interference of an absorptive and a gain resonance to obtain an enhanced index with vanishing absorption. As shown in Fig. 1(a), a straightforward way to realize such an interference is to have two different two-level transitions. These two transitions can either be in the same atom or can belong to two different atomic species. Such a multiple two-level scheme

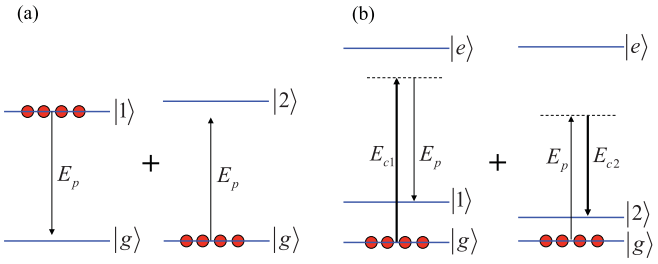

FIG. 1. (Color online) The interference of an absorptive resonance and an amplifying resonance can lead to an enhanced refractive index with vanishing absorption. (a) Shows the most straightforward way to achieve such an interference. Due to various difficulties, the scheme in (a) is not practical. (b) Shows an equivalent scheme using Raman transitions induced by two control lasers, E_{c1} and E_{c2}. By changing the excitation configuration from the ground level, a Raman resonance can be made amplifying or absorptive for the probe beam E_p.

has not yet been realized in practice since it is difficult to find two different transitions with close and easily tunable resonance frequencies. Furthermore, due to collisional energy exchange, it is difficult to maintain population inversion in one transition but not the other [27]. We recently proposed that such a multiple two-level scheme can be realized by using Raman resonances in far-off resonant atomic systems [30,31]. As shown in Fig. 1(b), with an atom starting in the ground state $|g\rangle$, a Raman transition involves absorption of one photon and emission of another photon of different frequency such that the two-photon resonance condition is satisfied. The laser beams that are involved can be very far detuned from the excited state $|e\rangle$. By changing the excitation configuration from the ground level ($E_{c1}E_p^*$ vs $E_pE_{c2}^*$), a Raman resonance can be made amplifying or absorptive for the probe laser. This scheme circumvents the difficulties of the original scheme of Fig. 1(a). The two Raman transition frequencies can be arbitrarily different since we have the freedom to choose the frequencies of the control lasers, E_{c1} and E_{c2}. There is also no population inversion requirement and the system remains mostly in the ground state at all times.

A detailed description of our scheme and the related formalism can be found in Refs. [30,32]. Figure 2 shows representative plots for the real part, χ', and the imaginary part, χ'', of the susceptibility as a function of the frequency of the probe laser beam. The refractive index is related to the real part through the relation $n = \sqrt{1+\chi'}$ and the imaginary part determines the loss or gain on the beam. In Fig. 2, for simplicity, the two Raman transitions are assumed to have equal parameters including identical Raman linewidth of γ. In the plots, the spacing between the two Raman transitions is $\Delta = 10\gamma, 5\gamma, \gamma$, respectively. At the midpoint between the two resonances, the beam experiences an enhanced refractive index with vanishing absorption.

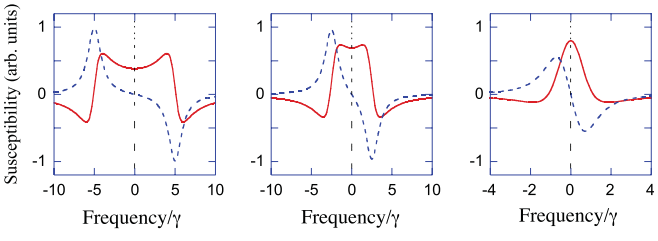

FIG. 2. (Color online) The real part χ' (solid line) and the imaginary part χ'' (dashed line) of the susceptibility of the probe laser for Raman transitions separated by $\Delta = 10\gamma$, 5γ, and γ, respectively. At the midpoint between the resonances, there is destructive interference in the imaginary part of the susceptibility yielding vanishing absorption. At the same point, the real part of the susceptibility obtains a large value due to constructive interference, which simultaneously yields an enhanced refractive index.

The strength of the Raman resonances, and therefore the value of the refractive index, is controlled by the intensity of the control laser beams. A natural question to ask then is how much can the refractive index of the medium be increased using this approach. It is now understood that for a sufficiently large control laser intensity, the medium will have its maximum possible index (as if the probe beam were tuned very close to the single-photon electronic resonance with state $|e\rangle$), and this refractive index is obtained while maintaining vanishing absorption. This limit is achieved when the Rabi frequencies of the control lasers are $\Omega_{c1} \approx \Omega_{c2} \approx \Delta\omega\sqrt{\gamma/\Gamma}$. Here, $\Delta\omega$ is the large single-photon detuning from the excited state, and Γ is the total width of the excited state (radiative + collisional + Doppler). All of these results were also derived by Kocharovskaya and colleagues [31].

One of the key questions in this technique is the amount of noise added to the probe beam while propagating through such an enhanced index medium. At the midpoint between the resonances, although the beam experiences vanishing absorption, the beam becomes noisier due to spontaneously emitted photons. Recently, by using the Heisenberg-Langevin noise operator approach, we have estimated the number of noise photons added to the beam [42]. We have shown that, at the point of vanishing absorption, roughly $(n-1)(2\pi/\lambda_0)L$ noise photons are added to the beam at the end of a medium of length L. For $n = 2$ and $L = 1$ mm, the number of noise photons at the point of vanishing absorption is about 10^4 and is negligible for even a nanojoule-level weak probe beam.

II. EXPERIMENTAL SCHEMATIC

Figure 3 shows the simplified setup for our experiments. We work with a triple layer magnetically shielded and temperature controlled vapor cell containing natural abundance Rb (28% ^{87}Rb, 72% ^{85}Rb). The vapor cell is $L = 1$ mm long and contains 10 torr of nitrogen (N_2) as a buffer gas. For Raman transitions between the hyperfine ground states, we utilize far-off resonant excitation through the excited electronic state $5P_{3/2}$ (D_2 line) near a wavelength of $\lambda = 780.2$ nm. The three experimental beams, E_p, E_{c1}, and E_{c2}, are derived from a single master external cavity diode laser with a linewidth of about 0.5 MHz. The output of this master laser is appropriately shifted by three high-frequency acousto-optic modulators (AOM) in parallel to produce the desired relative frequency spacing between the beams. The relative frequency stability between the experimental beams is at the 1-Hz level. After the AOMs, the control beams are amplified by tapered amplifiers to achieve the required power levels. The frequency of each of the three laser beams can be tuned by changing the modulation frequency of the AOMs. This setup gives us complete control

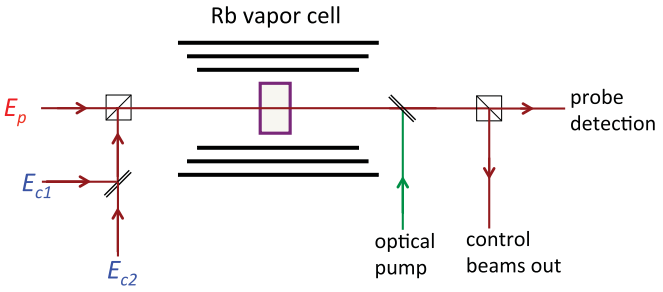

FIG. 3. (Color online) Simplified experimental schematic. The experiment is performed in a magnetically shielded, natural abundance Rb vapor cell with a length of $L = 1$ mm. The three experimental beams, E_p, E_{c1}, and E_{c2}, are obtained by appropriate frequency shifting and amplifying the output of a single master external cavity diode laser. After the cell, we separate the probe laser beam with a high extinction polarizer and perform our measurements. Some experiments utilize optical pumping lasers, which propagate in a direction opposite to the experimental laser beams.

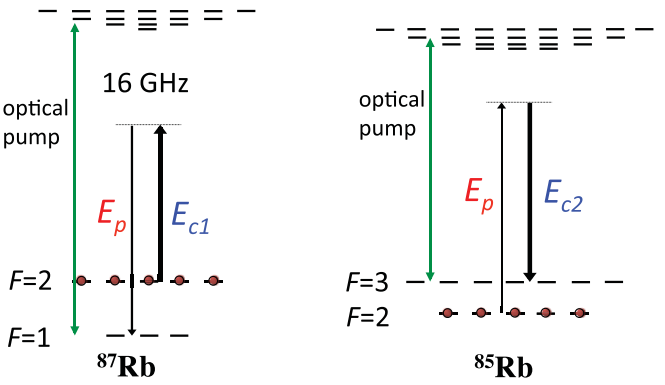

FIG. 4. (Color online) Refractive index enhancement using two Raman transitions in two isotopes of Rb. We start this experiment by pumping both of the atomic species to the $F = 2$ hyperfine level. This is achieved using two optical pump lasers locked to appropriate transitions. With the atoms pumped, we electromagnetically induce two Raman transitions, one in each isotope. A key issue with this scheme is the cross-coupling of the two optical pumping processes which results in a low value of the relative index.

over the position of the two Raman resonances. Further details regarding our laser system can be found in our previous publications [43,44]. The polarization of the probe beam is linear and orthogonal to the polarization of the two control laser beams. The three beams have collimated beam waists of $W_0 = 0.76$ mm at the vapor cell. Because our experiment is very sensitive to spatial mode purity, all three laser beams are spatially filtered using single-mode, polarization maintaining fibers before they are coupled to the cell. The probe laser has an optical power of a fraction of a mW and is much weaker than the control lasers (up to 50 mW each). For some experiments, we utilize additional optical pumping laser beams which are locked to appropriate transitions. These lasers are obtained from separate external cavity diode lasers whose outputs are also amplified by semiconductor tapered amplifiers. We are able to produce optical pumping power of about 70 mW at the cell.

As mentioned earlier, the two Raman transitions can either be in the same species or can belong to two different species. For our proof-of-principle experiment, we had used the two species setup of Fig. 4 [32]. We begin that experiment by optically pumping both of the atomic species to the $F = 2$ hyperfine state manifold. This is achieved using two optical pumping lasers locked to the $F = 1 \rightarrow F' = 2$ transition in ^{87}Rb and the $F = 3 \rightarrow F' = 3$ transition in ^{85}Rb, respectively. We run the experiment in a timing cycle where we optically pump the atoms for about 500 μs. We then turn off the optical pumping beams and turn on the probe and the control lasers. To avoid undesired time dynamics due to sharp edges, we turn on the three beams smoothly over about 10 μs and perform our measurements at the peak of the pulses. To determine the gain or the loss on the probe beam, we measure the intensity of the beam at the peak of its spatial profile using a pinhole placed immediately after the vapor cell. The key issue with such a two-species scheme is the cross coupling of the two optical pumping processes. The ^{87}Rb optical pumping laser tries to pump the ^{85}Rb atoms to the wrong F level and vice versa. As a result, the achieved enhancement of the refractive index is very low, $\Delta n \approx 2 \times 10^{-7}$.

In this paper, we will focus on the single-species scheme of Fig. 5. In this scheme, we use ^{85}Rb and optically pump to the $F = 3$ level. This configuration does not suffer from the cross-coupling of the two optical pumping processes. Furthermore, the required frequency span of the three experimental beams is smaller compared to the arrangement in Fig. 4. As a result, the scheme requires a smaller number of high-frequency AOMs which considerably simplifies the experimental setup. We have found the setup of Fig. 5 to be more robust than the two-species approach of Fig. 4, producing much higher values of the relative index. All of the data in the remainder of this paper will be presented for this single-species configuration.

We have experimentally found the scheme of Fig. 5 to be relatively insensitive to the presence of the optical pumping laser. The reason for this is that the intense control laser beams optically pump the atoms to the $F = 3$ hyperfine level themselves. For this case, the introduction of the optical pumping laser can increase the strength of each resonance slightly, by as much as 10%, but otherwise does not have a

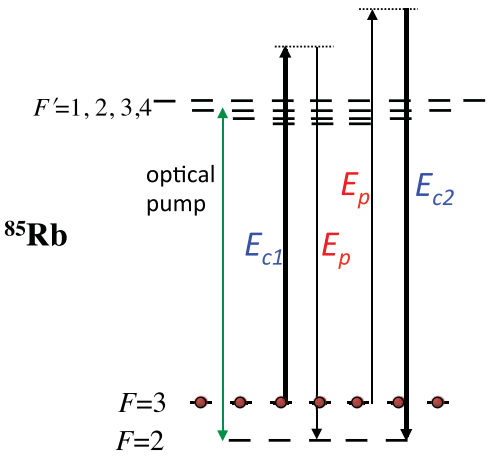

FIG. 5. (Color online) Refractive index enhancement in ^{85}Rb. We optically pump to the $F = 3$ level and induce two Raman transitions. The spacing between the $F = 2$ and $F = 3$ levels is 3.035 GHz. This configuration has significant advantages over that of Fig. 4.

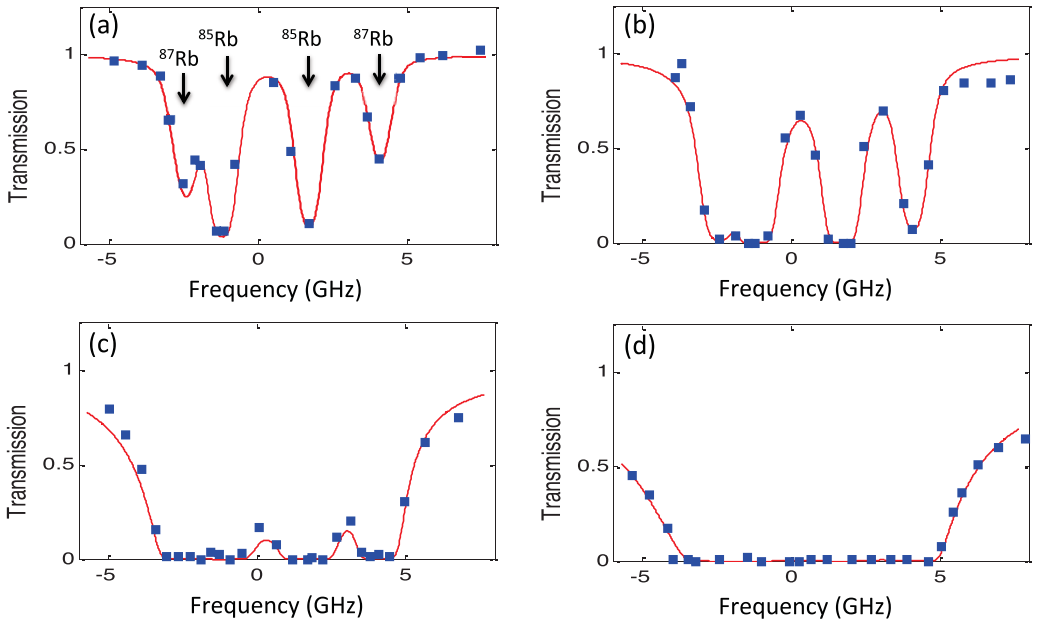

FIG. 6. (Color online) Normalized probe transmission through the cell as its frequency is scanned across the D_2 line (one unit indicates 100% transmission). The cell temperatures are $T = 96, 115, 144$, and 163 °C for plots (a) through (d), respectively. The vapor pressure model gives $N = 4.4 \times 10^{12}, 1.5 \times 10^{13}, 7.1 \times 10^{13}$, and 1.8×10^{14} cm^{-3} at these temperatures. The solid lines are numerical calculations without any adjustable parameters that use these density values and known dipole matrix elements, and Doppler- and pressure-broadened linewidths of the excited levels. The good agreement between the data and the calculation shows that the estimated values of the density are reasonably accurate.

significant effect on the experimental results. In this scheme, to allow sufficient time for optical pumping with the control lasers, we typically turn on these beams about 100 μs before the probe laser beam.

III. EXPERIMENTAL RESULTS

A. Spectroscopy of the D_2 line

In our experiments, it is important to know the density of the vapor as accurately as possible. To accomplish this, we have performed absorption spectroscopy of the D_2 line by measuring the transmission of a weak probe laser beam propagating alone (without the control lasers) while its frequency is scanned across the resonance. As we discuss below, we use the change in these absorption curves to characterize the efficiency of optical pumping to a specific F level. We perform the absorption spectroscopy experiments at different vapor cell temperatures as measured by an attached thermocouple. The vapor cell temperature is stabilized to within ±0.1 °C using a PID feedback loop which controls the current of the high-resistance heating wires. Figure 6 shows the probe transmission vs frequency at cell temperatures of $T = 96, 115, 144$, and 163 °C. As the vapor temperature is increased, the absorption window becomes saturated due to the high atomic density. In Fig. 6(a), the central two features are due to ^{85}Rb, whereas the outer features are due to ^{87}Rb. The frequency spacing between the features corresponds to the hyperfine splitting of the ground electronic states, 3.035 GHz for ^{85}Rb and 6.834 GHz for ^{87}Rb. The hyperfine structures of the excited electronic states are not resolved. The solid red lines in Fig. 6 are absorption calculations without any adjustable parameters. We use the vapor pressure model of Ref. [45] to estimate the density and include known dipole matrix elements and Doppler- and pressure-broadened linewidths of the excited hyperfine levels [46,47]. There is very good agreement between the calculations and the experimental data. This confirms that the vapor density given by the vapor pressure model is reasonably accurate. The model gives $N = 4.4 \times 10^{12}$ cm^{-3} for (a), 1.5×10^{13} cm^{-3} for (b), 7.1×10^{13} cm^{-3} for (c), and 1.8×10^{14} cm^{-3} for (d).

B. Optical pumping

For the refractive index enhancement scheme, it is critical that the atoms are optically pumped to the required hyperfine level, either with the separate optical pumping laser or with the intense control laser. To investigate the efficiency of optical pumping to a specific hyperfine level, we study the change in the absorption spectrum of the probe laser beam in the presence of an optical pumping laser locked to the appropriate transition. Figure 7 shows the transmission of a weak probe beam through the cell with (solid circles) and without (solid diamonds) an optical pumping laser locked to the $F = 2 \rightarrow F' = 3$ transition of the D_2 line in ^{87}Rb. Plot (a) is obtained for a cell temperature of $T = 96$ °C ($N = 4.4 \times 10^{12}$ cm^{-3}) and plot (b) is obtained for a cell temperature of $T = 163$ °C ($N = 1.8 \times 10^{14}$cm^{-3}). The optical pumping laser pumps both isotopes to the lower energy hyperfine level and, as a result, higher frequency features of the absorption spectrum become more dominant. In plot (b), even though the spectrum is very saturated, the shift of the whole absorption spectrum to higher frequencies is evident.

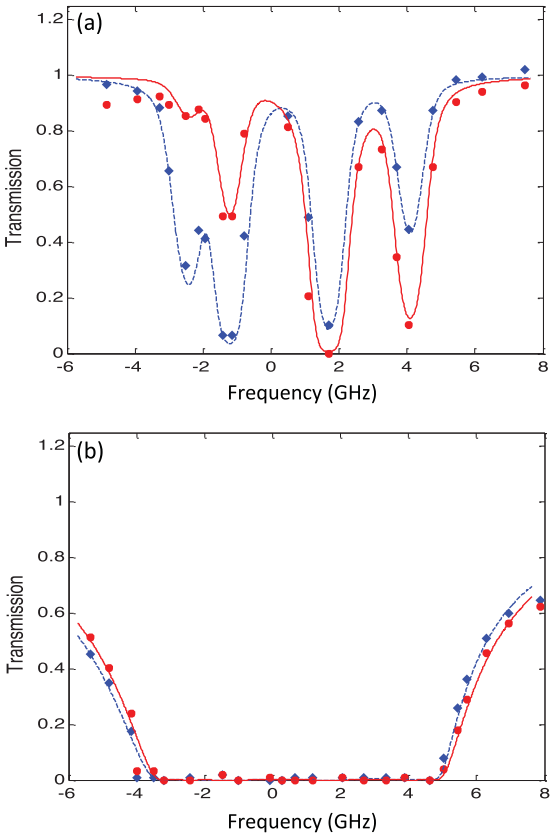

FIG. 7. (Color online) Normalized probe transmission through the cell with (solid circles) and without (solid diamonds) an optical pumping laser for cell temperatures of (a) $T = 96\ ^{\circ}\mathrm{C}$ ($N = 4.4 \times 10^{12}\ \mathrm{cm}^{-3}$) and (b) $T = 163\ ^{\circ}\mathrm{C}$ ($N = 1.8 \times 10^{14}\ \mathrm{cm}^{-3}$). The optical pumping laser pumps both isotopes to their lower energy hyperfine level resulting in stronger higher frequency features of the spectrum.

From the data of Fig. 7, we can infer the percentage of the atoms that are pumped from the upper hyperfine level to the lower hyperfine level in both isotopes. The solid lines in Fig. 7 are fits to the data, using the known densities, transition strengths, and linewidths, and varying the percentage of the atoms that are pumped. For example, in plot (a), the fit to the solid circles assumes 90% of ^{87}Rb atoms that were in $F = 2$ are pumped to $F = 1$, and 80% of ^{85}Rb atoms that were in $F = 3$ are pumped to $F = 2$. By changing the parameters of the optical pumping laser, such as its frequency and its power, the pumping efficiency can be optimized for each of the isotopes. Figure 8 shows the percentage of atoms pumped from $F = 2$ to $F = 1$ for ^{87}Rb as the vapor density is increased. We pump a large fraction of atoms for densities as high as 1.2×10^{14} cm^{-3}, above which the pumping efficiency drops sharply. We observe similar results for ^{85}Rb, and also for pumping from lower hyperfine to upper hyperfine levels (not shown in Fig. 8). A drop in pumping efficiency with increasing density is expected since various depumping mechanisms, such as spin-exchange collisions and radiation trapping, become more pronounced. We do not observe such a sharp drop in pumping efficiency in our calculations, however, and are currently working toward understanding this discrepancy. To our knowledge, the data of Fig. 8 demonstrates the highest alkali vapor density where such F level optical pumping has been observed.

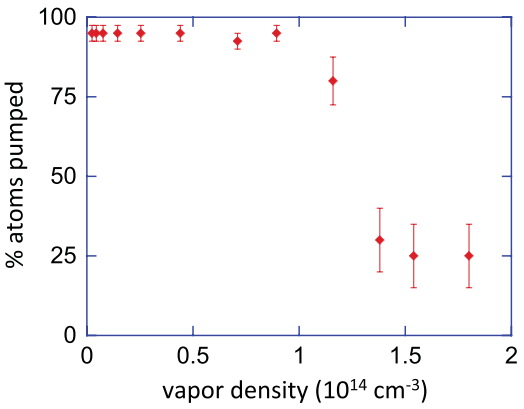

FIG. 8. (Color online) The percentage of atoms pumped from $F = 2$ to $F = 1$ for ^{87}Rb as the vapor density is increased. The optical pumping laser is locked to the $F = 2 \rightarrow F' = 3$ transition of the D_2 line in ^{87}Rb. We pump a large fraction of atoms for densities as high as 1.2×10^{14} cm^{-3}, above which the pumping efficiency drops sharply. We observe similar results for ^{85}Rb, and also for pumping from lower hyperfine to upper hyperfine levels (not shown).

C. Individual Raman resonances

We next discuss observing individual gain and absorption Raman resonances. Figures 9(a) and 9(b) show the individual gain and absorption resonances that were obtained at a density of 1.4×10^{14} cm^{-3}. It is important to note that we are operating at a density that is about two orders of magnitude larger than the densities used in typical vapor-cell EIT experiments [48,49]. We observe a peak gain of a factor of 10 and a peak absorption of a factor of 13 with sub-MHz Raman linewidths. For this data, we use only one control laser at a time [i.e., the control laser for the absorption (gain) transition is blocked while recording the gain (absorption) data]. The data are taken at a single-photon detuning of about 7 GHz from the excited electronic state. We estimate that the residual two-photon Doppler broadening contribute 187 kHz to the observed linewidth, whereas the broadening due to the time duration of the probe pulse is ≈ 10 kHz.

As we discuss in detail below, when we combine the two resonances, we observe a reduced strength of each resonance, in particular the absorption resonance, due to various cross-coupling mechanisms. We believe, however, most of these cross coupling mechanisms are technical in nature and may possibly be remedied in the future. It is, therefore, instructive to estimate the refractive index that would be achieved if the two resonances could be combined while retaining their original strength. Figure 9(c) shows the inferred real and imaginary parts of the refractive index when the two transitions of Figs. 9(a) and 9(b) are combined. The maximum inferred relative index at the point of vanishing absorption is $\Delta n = 1.5 \times 10^{-4}$. As we discuss below, in our current experiment, we obtain a relative index of $\Delta n \approx 0.4 \times 10^{-4}$ with low absorption (i.e., about a factor of 4 lower than this ideal limit). In Fig. 9(c), we plot the change in the refractive index due to the Raman transitions only (i.e., the background

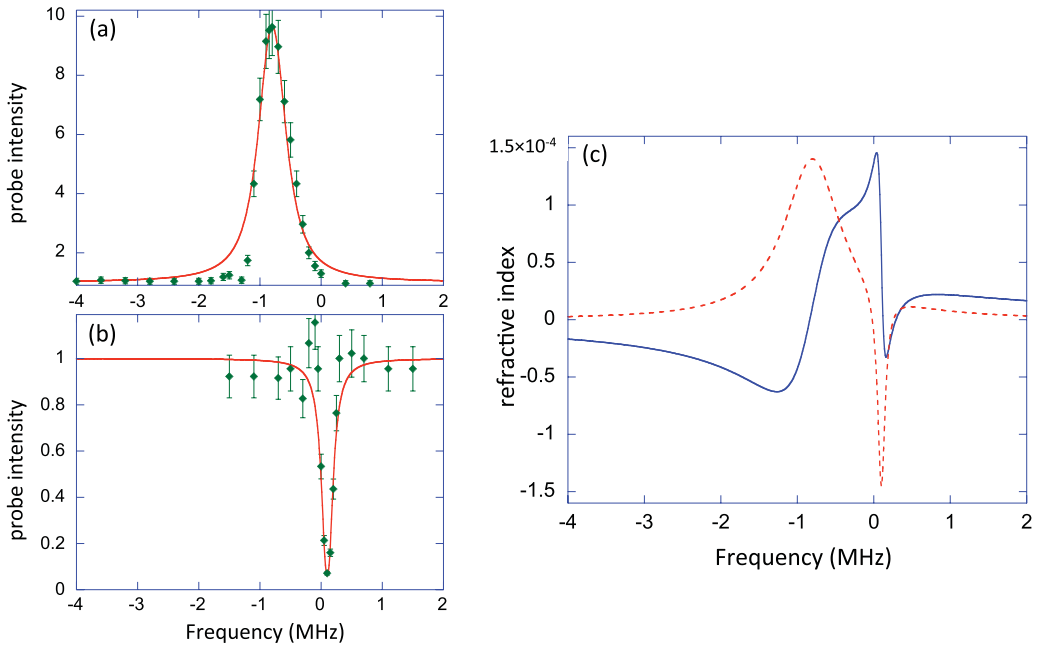

FIG. 9. (Color online) (a) The normalized transmitted intensity (I_{out}/I_{in}) of the probe laser as its frequency is scanned across the gain resonance for a cell length of $L = 1$ mm. We observe a peak gain of factor of 10. The probe (E_p) and control laser (E_{c1}) configuration is as shown in Fig. 5. (b) The transmitted intensity as the probe laser is scanned across the absorption resonance showing a peak absorption of a factor of 13. For this particular data, the E_p and E_{c2} configuration is slightly different than that shown in Fig. 5. (c) The inferred real (solid line) and imaginary (dashed line) parts of the relative index due to the Raman transitions only if the two transitions were combined while retaining their original strength.

refractive index of the vapor is not included). We estimate the background relative index of the vapor at this density to be -3.7×10^{-4}.

We have investigated the dependence of the individual resonances on various experimental parameters. For example, Fig. 10 shows the peak intensity gain achieved while the probe laser frequency is scanned across the gain resonance as the vapor temperature is varied. We observe an increase in the peak gain up until a temperature of $T \approx 155$ °C (corresponding to an atomic density of $N \approx 1.4 \times 10^{14}$ cm^{-3}), beyond which the gain saturates. The saturation is most likely due to the reduction in the efficiency of optical pumping as shown in Fig. 8 or due to the power broadening of the Raman transition as we discuss below. Because we are using a Pyrex vapor cell, we cannot increase the cell temperature much further than 165 °C since at higher temperatures Rb starts to chemically interact with the cell walls.

Figure 11 shows the strength of the gain resonance as the single-photon detuning of the laser beams from the D_2 line is varied at an atomic density of $N \approx 1.4 \times 10^{14}$ cm^{-3}. We find the optimal operating point to be about 7 GHz detuned from the D_2 line. Single-photon detunings significantly smaller than 7 GHz suffer from single-photon probe absorption due to the

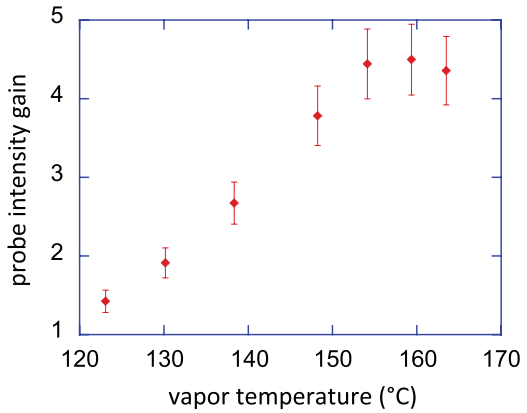

FIG. 10. (Color online) The peak intensity gain for the probe laser beam as the vapor temperature is varied. The highest gain is obtained for a temperature of $T \approx 155$ °C, which corresponds to an atomic density of $N \approx 1.4 \times 10^{14}$ cm^{-3}.

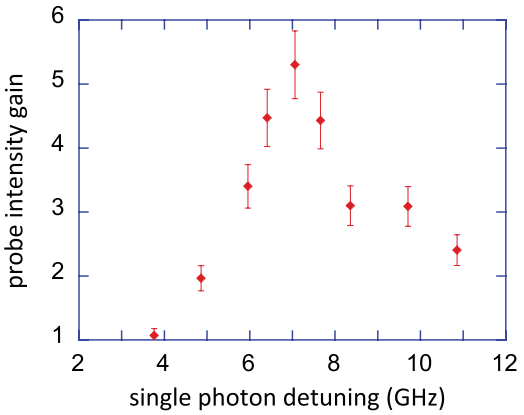

FIG. 11. (Color online) The peak intensity gain for the probe laser beam as the single-photon detuning from the D_2 line is varied. The highest gain is obtained for a detuning of about 7 GHz.

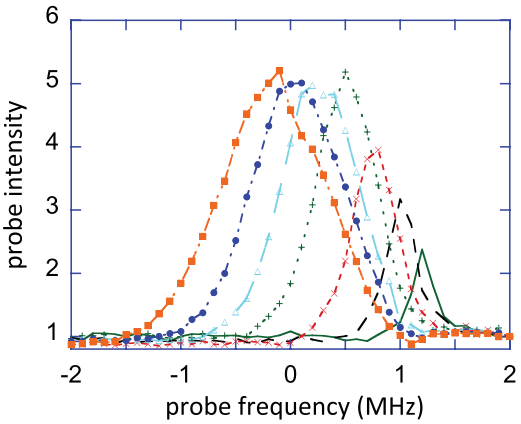

FIG. 12. (Color online) The normalized transmitted probe intensity (I_{out}/I_{in}) as its frequency is scanned across the gain resonance for a control laser (E_{c1}) power of 18 mW (solid line), 39 mW (dashed line), 64 mW (crosses), 93 mW (pluses), 120 mW (open triangles), 143 mW (solid circles), and 165 mW (solid diamonds). As the control laser power is increased, the strength of the Raman transition increases up to a certain control power level and then saturates. The shift and the broadening of the Raman transition are also clearly observed. The shift is due to the AC stark shift of the hyperfine levels, which results from the high intensity of the control laser.

large optical depth. Detunings significantly larger than 7 GHz suffer from reduced Raman coupling and also from the optical power limitation of the control laser beams. A detuning of 7 GHz seems to be the optimal point where single-photon absorption is small (about five percent) yet a sufficiently large Raman coupling is maintained. We have investigated the dependence of the absorption resonance on the variation of these parameters. We have found results comparable to those shown in Figs. 10 and 11.

Figure 12 shows the observed Raman gain resonances as the probe frequency is scanned for varying levels of control laser (E_{c1}) power. These data are obtained for optimal values of single-photon detuning ($\approx$7 GHz) and the atomic density ($N \approx 1.4 \times 10^{14}$ cm^{-3}). The shift and the broadening of the Raman transition is clearly observed as the control laser power is increased. Figure 13 summarizes the data of Fig. 12. Plot (a) shows the peak probe intensity gain for a range of control laser powers. The observed gain increases up to a control laser power of about 100 mW and then saturates (the optimization data of Figs. 10 and 11 are obtained with a control power value of approximately 100 mW). Figure 13(b) shows the shift of the Raman transition as the control laser power is increased. The shift is a result of the difference in the AC Stark shifts of the lower and upper hyperfine levels. The solid line is the calculated shift of the Raman transition using the known dipole matrix elements [45] and without any adjustable parameters (i.e., all parameters that we use in the calculation including the size of the beams are experimentally measured). It appears that the calculations overestimate the Raman transition shift by about 30%. The reason for the discrepancy is likely a slight spatial misalignment of the probe laser beam from the center of the control lasers.

Figure 13(c) shows the full width at half maximum (FWHM) of the Raman transition as the control laser power is varied. The solid line is a numerical calculation without any adjustable parameters. The observed power broadening of the Raman transition is much larger than what the calculation indicates. This broadening is a major limitation of the current experiments since it results in the saturation of the Raman transition for control powers exceeding 100 mW. Currently, we do not understand the physical mechanisms behind this broadening. We speculate that the broadening may possibly be caused by alkali dimer formation and dimer resonances coming into play [50,51].

D. Combining the two resonances

As mentioned above, when we combine the Raman gain and absorption resonances, we observe a reduced strength of each resonance. This is due to various cross-coupling processes, such as the additional control laser beam causing further Stark shift and broadening of each resonance. Another issue is that when the two transitions are combined, we have to work in a restricted parameter space for each transition. For example, the single-photon detunings for the Raman gain and absorption resonances are different by the ground-state hyperfine splitting

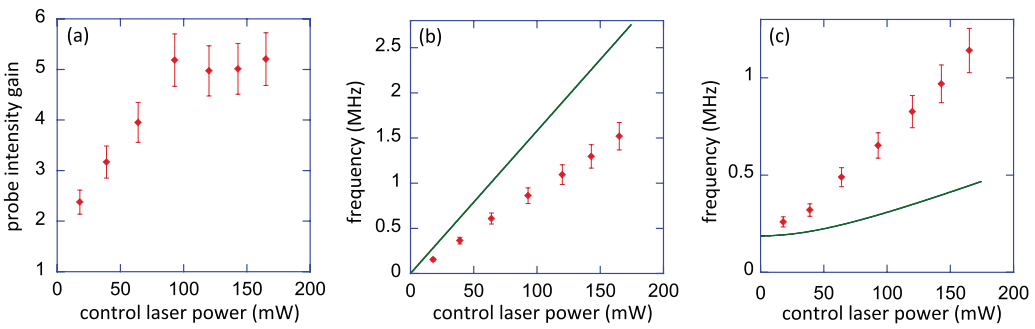

FIG. 13. (Color online) (a) The peak probe gain that is observed as the control laser power is increased. The gain increases up to a control laser power value of about 100 mW and then saturates. (b) The Raman resonance shift vs the control laser power. The shift is a result of the difference in AC Stark shifts of the lower and upper hyperfine levels. The solid line is a numerical calculation without any adjustable parameters. We observe reasonable agreement between the calculation and the experimental results. The discrepancy is likely due to a slight misalignment of the probe laser beam from the center of the control lasers. (c) The full width at half maximum (FWHM) of the Raman transition as the control laser power is varied. The solid line is a numerical calculation without any adjustable parameters. The observed power broadening of the Raman transition is much larger than what the calculation indicates.

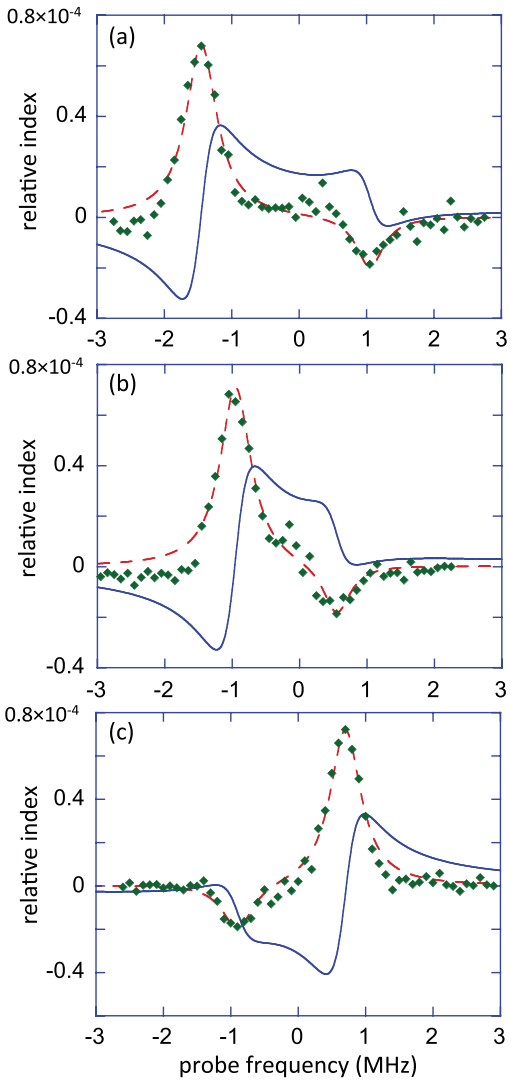

FIG. 14. (Color online) The real (solid lines) and the imaginary (data points and dashed lines) parts of the refractive index when the two Raman resonances are combined. The dashed lines are fits to the data that assumes each Raman resonance to have a Lorentzian lineshape. The solid lines are the calculated real part of the refractive index based on these fits. In plots (a) and (b) the gain resonance occurs before the absorption resonance whereas in plot (c) the situation is reversed. We observe a change in refractive index of $|\Delta n| \approx 0.4 \times 10^{-4}$ with low absorption.

of 3.035 GHz. As a result, we cannot have the optimal detuning of 7 GHz for each transition. The reduction of the transition strength is particularly pronounced for the Raman absorption resonance.

Figure 14 shows the observed combined gain and absorption resonances as the probe frequency is scanned. Here we measure the probe intensity absorption or gain at the end of the cell ($I_{\text{out}}/I_{\text{in}}$) and then back-calculate the imaginary part of the refractive index using the known cell length of $L = 1$ mm. The dashed lines are fits to the data that assume each Raman resonance to have a Lorentzian lineshape. The three adjustable parameters in the fits are the strength, the position, and the width of each Raman resonance. We observe good agreement between the fits and the experimental data. From these fits, we evaluate the real part of the Lorentzian curves and calculate the real part of the refractive index (the solid lines in Fig. 14). By tuning the frequencies of the control laser beams, we can control the position of the Raman resonances as the probe laser frequency is scanned. In plots (a) and (b) the gain resonance occurs before the absorption resonance whereas in plot (c) the situation is reversed. As a result, in plots (a) and (b) we observe refractive index enhancement with vanishing absorption, whereas in plot (c) we observe refractive index reduction with vanishing absorption. For all three cases, we observe a change in refractive index of $|\Delta n| \approx 0.4 \times 10^{-4}$ with low absorption.

E. Four-wave mixing

It is well known that once a Raman coherence is produced, additional frequencies can be generated in the medium due to four-wave mixing (FWM) [52,53]. These new sidebands can substantially interfere with the Raman gain and absorption on the probe laser beam. This effect becomes especially important when the Raman gain (loss) on the probe beam becomes larger than $\exp[1]$ ($\exp[-1]$). We look for this effect using a scanning fabry-perot interferometer at the output of the cell to see if there are any new frequencies being generated. We do not observe any significant FWM generation due to the following reasons: (i) As mentioned before, at densities exceeding 10^{14} cm^{-3}, the optical depth becomes very large for our 1-mm-long vapor cell. As a result, there is a wide window of frequencies with substantial single-photon absorption. For our typical experimental parameters, the FWM sideband due to Raman gain resonance (at a frequency of $2\omega_{c1} - \omega_p$) is well within the absorption curve. As a result, the FWM sideband does not significantly amplify and interfere with the Raman gain process for the probe laser beam. (ii) For these conditions, the FWM sideband due to Raman absorption resonance (at a frequency $2\omega_{c2} - \omega_p$) is typically sufficiently far detuned from the D_2 line that we do not observe significant sideband amplification.

To summarize, to date we have been able to control this issue and FWM is not the limiting factor for our current experimental parameters. However, we note that this issue may limit the maximum achievable length of the index-enhanced medium for future experiments.

IV. FUTURE PROSPECTS

A. Maximum refractive index

One of the key questions to ask is what is the largest value of the refractive index that can be achieved in Rb? As mentioned before, for sufficiently large control laser intensities, the medium will exhibit its largest possible refractive index, that is, as if the probe beam were tuned close to the single-photon excited state resonance. Figure 15 shows the maximum achievable relative index of Rb as a function of density for a hot vapor. The maximum relative index increases linearly up to a density of about 10^{15} cm^{-3} and then saturates at $\Delta n = 0.4$. The saturation is fundamental and is caused by the pressure broadening of the excited electronic state $|e\rangle$ [31,54–57]. One of the key goals would be to achieve the predicted maximum index experimentally. The refractive

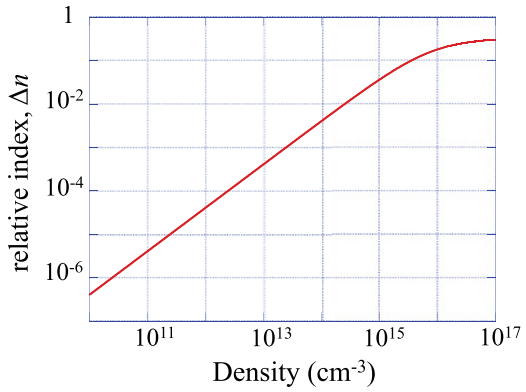

FIG. 15. (Color online) The maximum relative index for a hot Rb atomic vapor. The index increases linearly up to a density of about 10^{15} cm^{-3} and then saturates at a value of $\Delta n \approx 0.4$.

index that we have achieved in our current experiment is about a factor of 30 lower than the ideal prediction of Fig. 15. We note that observing the maximum refractive index predicted by Fig. 15 will likely be a challenging experiment. Many second-order issues in high-density alkali vapors, such as radiation trapping and dimer formation, will likely need to be carefully investigated before such high values of the refractive index are obtained.

B. Short vapor cells

To fully understand the limitations of the experiment, we plan to explore index enhancement using shorter vapor cells. The main motivation for using shorter cells is that at atomic densities 10^{15} cm^{-3}, a 1-mm-long cell becomes very thick optically, with an on-resonance optical depth exceeding 100. As a result, many second-order issues, such as radiation trapping, are greatly amplified. We have recently acquired vapor cells with a cell length of $L = 30$ μm and started using these cells in our experiment. Figure 16 shows a D_2-line absorption spectrum for the probe laser beam without any control lasers at a cell temperature of $T = 163$ °C. The solid line is a theoretical calculation without any adjustable

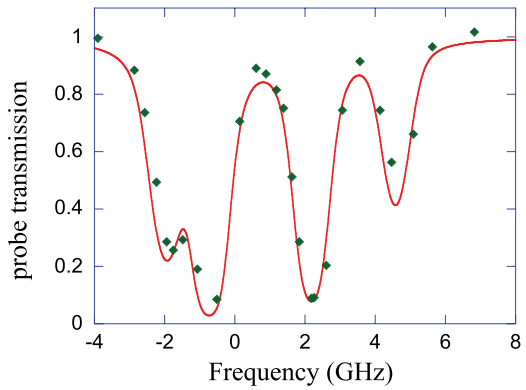

FIG. 16. (Color online) The probe transmission as its frequency is scanned across the D_2 line for a cell length of $L = 30$ μm and an atomic density of 2×10^{14} cm^{-3}. The two outer features are due to ^{87}Rb, whereas the two inner features are due to ^{85}Rb. The solid line is a calculation without any adjustable parameters.

parameters using the known line strengths and the atomic density calculated by the vapor pressure model of Ref. [45]. We observe good agreement with the observed data and the calculation. Our next immediate goal is to observe gain and absorption Raman resonances with these short vapor cells and to attempt to achieve higher relative indices.

C. Pyrex vs sapphire cells

Currently we are using vapor cells made of pyrex, and as a result, we cannot explore temperatures above 170 °C and thus densities exceeding 10^{15} cm^{-3}. This is because Rb starts to chemically interact with the cell walls at high temperatures. In future investigations, one could use sapphire vapor cells to eliminate this problem. We note that reflection spectroscopy of Rb at densities as high as 10^{17} cm^{-3} is routinely performed using sapphire cells [58–61].

D. D_1 vs D_2 line

As mentioned before, we have been performing the index enhancement experiments using the D_2 line in Rb. We initially chose this transition because of the availability of high-power tapered amplifiers near the D_2 line transition wavelength of 780 nm. However, it is well known that using the D_1 line has several advantages over the D_2 line [62]. For example, for the $D1$ line excitation in ^{85}Rb, all of the excited levels ($F' = 2$ and $F' = 3$) contribute to the Raman process. In contrast, the $F' = 1$ and $F' = 4$ levels of the D_2 line do not induce Raman coupling; they only produce background single-photon absorption resonances. These resonances are quite detrimental for near-resonance experiments such as EIT since they produce absorptive features that cannot be rendered transparent. For refractive index enhancement, these background resonances contribute to many undesired effects, such as power broadening of the Raman transitions and AC Stark shifts. To avoid such effects, future experiments may utilize the D_1 line. Tapered amplifiers have recently become available at the D_1 line transition wavelength of 795 nm.

E. Ultracold atoms

Ultracold atomic clouds have significant advantages over hot vapor cells for implementing refractive index enhancement. One key advantage is that the laser beams need not be collinear since there is negligible Doppler broadening. This allows the focusing of the beams to tight spots, which greatly reduces the optical power requirement for the control lasers. Atoms that are trapped in optical dipole traps show considerable promise for studies of refractive index enhancement. We note that current laser cooling and trapping techniques allow atomic densities exceeding 10^{15} cm^{-3} in a dipole trap [without the need for a Bose-Einstein condensate (BEC)] [63,64].

V. CONCLUSIONS

In conclusion, we have presented a detailed investigation of an approach for manipulating the refractive index of an atomic vapor while maintaining vanishing absorption. The approach relies on the interference of two Raman resonances, one amplifying and one absorptive in nature. We have

successfully performed experiments at Rb densities as high as 1.8×10^{14} cm^{-3}, which is two orders of magnitude larger than alkali densities used in typical EIT experiments. Our experiments demonstrated a refractive index change of about $\Delta n \approx 10^{-4}$, which is too small to have practical applications at this stage of development. However, we believe these experiments set the stage for future experiments in which the change in the refractive index could be of order unity. Currently the main limitation of our experiments is the unexplained power broadening of the Raman transition.

Extension of these ideas to solid-state materials is of great interest. As discussed in detail by Kocharovskaya and colleagues [65,66], using ideas such as coherent control of excited state absorption, one can manipulate the refractive index of solids with vanishing absorption. Using these techniques, it may be possible to obtain very large refractive indices, possibly approaching $n \approx 10$, opening an array of exciting applications. One could, for example, construct highly efficient optically controlled optical devices.

It has recently been predicted that when our index manipulation scheme is coherently coupled to a strong magnetic-dipole transition, one can obtain a negative refractive index with vanishing absorption [67,68]. The key advantage of this approach is that the scheme does not require the simultaneous presence of a strong electric-dipole and a strong magnetic-dipole transition at exactly the same wavelength [69–72]. A preliminary study of rare earth atomic species has revealed that the idea may possibly be experimentally implemented in atomic erbium (Er) or dysprosium (Dy) [68]. The concept of negative refraction, which was first predicted by Veselago more than four decades ago [73], has recently emerged as an exciting field of science [74–83]. Although the interest in these materials remained only a scientific curiosity for a long time, it is now understood that negative refraction may have important and far-reaching practical consequences, such as the construction of perfect lenses [84]. Although there are open questions, in the future, it may be possible to perform experiments similar to those discussed above in rare earth atoms and to investigate the possibility of achieving negative refraction with low absorption in the optical region of the spectrum.

ACKNOWLEDGMENTS

We thank Josh Weber for many helpful discussions and assistance with the experiment, and Tyler Green and Brett Unks for contributions in the early stages of this project. This work was supported by the Air Force Office of Scientific Research, Wisconsin Alumni Research Foundation, and start-up funds from the University of Wisconsin-Madison.

[1] M. O. Scully and M. S. Zubairy, *Quantum Optics* (Cambridge University Press, Cambridge, 1997).
[2] S. E. Harris, Phys. Today **50**, 36 (1997).
[3] O. Kocharovskaya and P. Mandel, Phys. Rev. A **42**, 523 (1990).
[4] A. Kasapi, M. Jain, G. Y. Yin, and S. E. Harris, Phys. Rev. Lett. **74**, 2447 (1995).
[5] M. Xiao, Y. Q. Li, S. Z. Jin, and J. Gea-Banacloche, Phys. Rev. Lett. **74**, 666 (1995).
[6] L. V. Hau, S. E. Harris, Z. Dutton, and C. H. Behroozi, Nature (London) **397**, 594 (1999).
[7] M. M. Kash, V. A. Sautenkov, A. S. Zibrov, L. Hollberg, G. R. Welch, M. D. Lukin, Y. Rostovtsev, E. S. Fry, and M. O. Scully, Phys. Rev. Lett. **82**, 5229 (1999).
[8] G. M. Gehring, A. Schweinsberg, C. Barsi, N. Kostinski, and R. W. Boyd, Science **312**, 895 (2007).
[9] M. Fleischhauer and M. D. Lukin, Phys. Rev. Lett. **84**, 5094 (2000).
[10] D. F. Phillips, A. Fleischhauer, A. Mair, R. L. Walsworth, and M. D. Lukin, Phys. Rev. Lett. **86**, 783 (2001).
[11] C. Liu, Z. Dutton, C. H. Behroozi, and L. V. Hau, Nature (London) **409**, 6819 (2001).
[12] I. Novikova, A. V. Gorshkov, D. F. Phillips, A. S. Sorensen, M. D. Lukin, and R. L. Walsworth, Phys. Rev. Lett. **98**, 243602 (2007).
[13] N. B. Phillips, A. V. Gorshkov, and I. Novikova, Phys. Rev. A **78**, 023801 (2008).
[14] H. Schmidt and A. Imamoglu, Opt. Lett. **21**, 1936 (1996).
[15] A. Imamoglu, H. Schmidt, G. Woods, and M. Deutsch, Phys. Rev. Lett. **79**, 1467 (1997).
[16] S. E. Harris and Y. Yamamoto, Phys. Rev. Lett. **81**, 3611 (1998).
[17] S. E. Harris and L. V. Hau, Phys. Rev. Lett. **82**, 4611 (1999).
[18] M. D. Lukin and A. Imamoglu, Phys. Rev. Lett. **84**, 1419 (2000).
[19] H. Wang, D. Goorskey, and M. Xiao, Phys. Rev. Lett. **87**, 073601 (2001)
[20] M. Yan, E. G. Rickey, and Y. Zhu, Phys. Rev. A **64**, 041801 (2001)
[21] H. Kang and Y. Zhu, Phys. Rev. Lett. **91**, 093601 (2003).
[22] D. A. Braje, V. Balic, S. Goda, G. Y. Yin, and S. E. Harris, Phys. Rev. Lett. **93**, 183601 (2004).
[23] V. Balic, D. A. Braje, P. Kolchin, G. Y. Yin, and S. E. Harris, Phys. Rev. Lett. **94**, 183601 (2005).
[24] P. Kolchin, S. Du, C. Belthangady, G. Y. Yin, and S. E. Harris, Phys. Rev. Lett. **97**, 113602 (2007).
[25] M. O. Scully, Phys. Rev. Lett. **67**, 1855 (1991).
[26] M. O. Scully and M. Fleischhauer, Phys. Rev. Lett. **69**, 1360 (1992).
[27] M. Fleischhauer, C. H. Keitel, M. O. Scully, C. Su, B. T. Ulrich, and S. Y. Zhu, Phys. Rev. A **46**, 1468 (1992).
[28] U. Rathe, M. Fleischhauer, S. Y. Zhu, T. W. Hansch, and M. O. Scully, Phys. Rev. A **47**, 4994 (1993).
[29] M. D. Lukin, S. F. Yelin, M. Fleischhauer, and M. O. Scully, Phys. Rev. A **60**, 3225 (1999).
[30] D. D. Yavuz, Phys. Rev. Lett. **95**, 223601 (2005).
[31] P. Anisimov and O. Kocharovskaya, in 38th Winter Colloquium on Physics of Quantum Electronics, Snowbird, Utah, 2008.
[32] N. A. Proite, B. E. Unks, J. T. Green, and D. D. Yavuz, Phys. Rev. Lett. **101**, 147401 (2008).
[33] A. S. Zibrov, M. D. Lukin, L. Hollberg, D. E. Nikonov, M. O. Scully, H. G. Robinson, and V. L. Velichansky, Phys. Rev. Lett. **76**, 3935 (1996).

[34] S. W. Hell and J. Wichmann, Opt. Lett. **19**, 780 (1994).
[35] T. A. Klar, E. Engel, and S. W. Hell, Phys. Rev. E **64**, 066613 (2001).
[36] E. Betzig, Opt. Lett. **20**, 237 (1995).
[37] C. Hettich, C. Schmitt, J. Zitzmann, S. Kuhn, I. Gerhardt, and V. Sandoghdar, Science **298**, 385 (2002).
[38] A. N. Boto, P. Kok, D. S. Abrams, S. L. Braunstein, C. P. Williams, and J. P. Dowling, Phys. Rev. Lett. **85**, 2733 (2000).
[39] M. D'Angelo, M. V. Chekhova, and Y. Shih, Phys. Rev. Lett. **87**, 013602 (2001).
[40] K. S. Johnson, J. H. Thywissen, N. H. Dekker, K. K. Berggren, A. P. Chu, R. Younkin, and M. Prentiss, Science **280**, 1583 (1998).
[41] S. J. Bentley and R. W. Boyd, Opt. Express **12**, 5735 (2004).
[42] D. D. Yavuz and N. A. Proite, Phys. Rev. A **78**, 053811 (2008).
[43] B. E. Unks, N. A. Proite, and D. D. Yavuz, Rev. Sci. Instrum. **78**, 083108 (2007).
[44] N. A. Proite, B. E. Unks, J. T. Green, and D. D. Yavuz, Phys. Rev. A **77**, 023819 (2008).
[45] Daniel A. Steck, [http://steck.us/alkalidata].
[46] M. D. Rotondaro and G. P. Perram, J. Quant. Spectrosc. Radiat. Transfer **57**, 497 (1997).
[47] M. V. Romalis, E. Miron, and G. D. Cates, Phys. Rev. A **56**, 4569 (1997).
[48] K. J. Jiang, L. Deng, and M. G. Payne, Phys. Rev. A **74**, 041803(R) (2006).
[49] P. K. Vudyasetu, R. M. Camacho, and John C. Howell, Phys. Rev. A **82**, 053807 (2010).
[50] T. Scholz, M. Schiffer, J. Welzel, D. Cysarz, and W. Lange, Phys. Rev. A **53**, 2169 (1995).
[51] L. K. Lam, T. Fujimoto, A. C. Gallagher, and M. M. Hessel, J. Chem. Phys. **68**, 3553 (1978).
[52] R. M. Camacho, P. K. Vudyasetu, and J. C. Howell, Nature Photonics **3**, 103 (2009).
[53] P. Londero, V. Venkataraman, A. R. Bhagwat, A. D. Slepkov, and A. L. Gaeta, Phys. Rev. Lett. **103**, 043602 (2009).
[54] H. vanKampen, A. V. Papoyan, V. A. Sautenkov, P. H. A. M. Castermans, E. R. Eliel, and J. P. Woerdman, Phys. Rev. A **56**, 310 (1997).
[55] K. Niemax, M. Movre, and G. Pichler, J. Phys. B **12**, 3503 (1979).
[56] K. Niemax and G. Pichler, J. Phys. B **8**, 179 (1975).
[57] J. Huennekens and A. Gallagher, Phys. Rev. A **27**, 1851 (1983).
[58] J. J. Maki, M. S. Malcuit, J. E. Sipe, and R. W. Boyd, Phys. Rev. Lett. **67**, 672 (1991).
[59] V. A. Sautenkov, H. van Kampen, E. R. Eliel, and J. P. Woerdman, Phys. Rev. Lett. **77**, 3327 (1996).
[60] H. van Kampen, V. A. Sautenkov, E. R. Eliel, and J. P. Woerdman, Opt. Commun. **180**, 81 (2000).
[61] H. Li, V. A. Sautenkov, Y. V. Rostovtsev, and M. O. Scully, J. Phys. B: At. Mol. Opt. Phys. **42**, 065203 (2009).
[62] M. Stahler, R. Wynands, S. Knappe, J. Kitching, L. Hollberg, A. Taichenachev, and V. Yudin, Opt. Lett. **27**, 1472 (2002).
[63] R. Newell, J. Sebby, and T. G. Walker, Opt. Lett. **28**, 1266 (2003).
[64] J. Sebby-Strabley, R. T. R. Newell, J. O. Day, E. Brekke, and T. G. Walker, Phys. Rev. A **71**, 021401(R) (2005).
[65] C. OBrien, P. M. Anisimov, Y. Rostovtsev, and O. Kocharovskaya, Phys. Rev. A **84**, 063835 (2011).
[66] C. O'Brien and O. Kocharovskaya, Phys. Rev. Lett. **107**, 137401 (2011).
[67] D. E. Sikes and D. D. Yavuz, Phys. Rev. A **82**, 011806(R) (2010).
[68] D. E. Sikes and D. D. Yavuz, Phys. Rev. A **84**, 053836 (2011).
[69] M. O. Oktel and O. E. Mustecaplioglu, Phys. Rev. A **70**, 053806 (2004).
[70] Q. Thommen and P. Mandel, Phys. Rev. Lett. **96**, 053601 (2006).
[71] J. Kästel, M. Fleischhauer, S. F. Yelin, and R. L. Walsworth, Phys. Rev. Lett. **99**, 073602 (2007).
[72] J. Kästel, M. Fleischhauer, S. F. Yelin, and R. L. Walsworth, Phys. Rev. A **79**, 063818 (2009).
[73] V. G. Veselago, Sov. Phys. Usp. **10**, 509 (1968).
[74] R. A. Shelby, D. R. Smith, and S. Shultz, Science **292**, 77 (2001).
[75] A. A. Houck, J. B. Brock, and I. L. Chuang, Phys. Rev. Lett. **90**, 137401 (2003).
[76] P. V. Parimi, W. T. Lu, P. Vodo, J. Sokoloff, J. S. Derov, and S. Sridhar, Phys. Rev. Lett. **92**, 127401 (2004).
[77] E. Cubukcu, K. Aydin, E. Ozbay, S. Foteinopoulou, and C. M. Soukoulis, Nature (London) **423**, 604 (2003).
[78] T. J. Yen, W. J. Padilla, N. Fang, D. C. Vier, D. R. Smith, J. B. Pendry, D. N. Basov, and X. Zhang, Science **303**, 1494 (2004).
[79] V. M. Shalaev, W. Cai, U. K. Chettiar, H. Yuan, A. K. Sarychev, V. P. Drachev, and A. V. Kildishev, Opt. Lett. **30**, 3356 (2005).
[80] S. Zhang, W. Fan, N. C. Panoiu, K. J. Malloy, R. M. Osgood, and S. R. J. Brueck, Phys. Rev. Lett. **95**, 137404 (2005).
[81] G. Dolling, C. Enkrich, M. Wegener, C. M. Soukoulis, and S. Linden, Opt. Lett. **31**, 1800 (2006).
[82] M. S. Rill, C. Plet, Michael Thiel, I. Staude, G. Freymann, S. Linden, and M. Wegener, Nat. Mater. **7**, 543 (2008).
[83] H. J. Lezec, J. A. Dionne, and H. A. Atwater, Science **316**, 430 (2007).
[84] J. B. Pendry, Phys. Rev. Lett. **85**, 3966 (2000).